High Temporal- and Spatial-Resolution Photographs of the "Christmas" Red-Green Auroras Taken Over Germany During a Main Phase of the 10–11 May 2024 ~~SYM-H = −518 nT~~ Superstorm

Bruce T. Tsurutani[1,*], Gurbax S. Lakhina[2,**], Rajkumar Hajra[3], Masatomi Iizawa[4], Yasuhito Narita[4,5], Richard B. Horne[6], Ingo von Borstel[7], Volker Bothmer[8,†], Karl-Heinz Glassmeier[7,5], Klaus Reinsch[8], Philipp Schulz[9], and Sami Solanki[5]

[1]Jet Propulsion Laboratory, California Institute of Technology, Pasadena, California, USA
[2]Indian Institute of Geomagnetism, Navi Mumbai, India
[3]CAS Key Laboratory of Geospace Environment, School of Earth and Space Sciences, University of Science and Technology of China, Hefei, People's Republic of China
[4]Institut für Theoretische Physik, Technische Universität Braunschweig, Braunschweig, Germany
[5]Max-Planck-Institut für Sonnensystemforschung, Göttingen, Germany
[6]British Antarctic Survey, Cambridge, England
[7]Institut für Geophysik und Extraterrestrische Physik, Technische Universität Braunschweig, Braunschweig, Germany
[8]Institut für Astrophysik und Geophysik, Georg-August-Universität Göttingen, Germany
[9]Fraunhofer-Institut für Schicht-und Oberflächentechnik IST, Braunschweig, Germany
[*]Retired, Pasadena, California, USA
[**]Retired, B-701, Neel Sidhi Towers, Sector-12, Vashi, Navi Mumbai, India
[†]Deceased, 23 April 2026

Correspondence: Y. Narita (y.narita@tu-braunschweig.de)

Abstract. The 10–11 May 2024 superstorm had three main phase steps with peak intensities SYM-H $= -183$ nT, -354 nT and -518 nT. During the second main phase a red and green aurora occurred over Braunschweig and Göttingen, Germany. The Braunschweig and Göttingen red and green auroral images were taken during intense substorms within the storm second main phase. The high-altitude red aurora displayed brightness streaks/rays, which continued to lower altitude green auroral brightness streaks/rays. Of the many postulated mechanisms for causing red auroras, it is concluded that high energy electron precipitation along the Earth's magnetic field lines was the main mechanism for both auroral streaks/rays. The plasmapause location estimated using the Dst index was $L \sim 2.6$, corresponding to the approximate L-shell of Braunschweig and Göttingen.

1 Introduction

One of the major long-standing mysteries in Space Weather and Space Physics is the physical cause or causes of red auroras. Red auroras occur at midlatitudes at altitudes of ∼200 km to ∼800 km during magnetic storms (Barbier, 1958; Roach and Marovich, 1959) where direct physical measurements are extremely difficult to make. See an excellent review by Shiokawa et al. (2005) for red auroras over Japan and Kozyra et al. (1993) for red auroras in general. What are needed to determine the physical causes of red auroras are measurements of suprathermal electrons, suprathermal ions, energetic electrons, kinetic

Alfvén waves and ion cyclotron waves to distinguish between the many theoretical hypotheses proposed for generating these types of auroras. Even though red auroras have been extensively studied since the 1960s, very few of the above measurements have been made to date. So, the science community has had to rely on theoretical arguments and any possible indirect information they can obtain. During the May 10–11 2024 superstorm there were no direct measurements of the causes of red or red-like auroras. All reports were "citizen science" reports. This article will also be a citizen science report.

There has been a recent superstorm of peak intensity SYM-H $= -518$nT on 10–11 May 2024 (Grandin et al., 2024; Hajra et al., 2024). Auroral viewings during this storm were reported from all over the world. Citizen-science auroral observations from >30 countries the aurora at geomagnetic latitudes ranging between 30° and 60° with a few observations from even lower latitudes (Grandin et al., 2024). The auroral emissions reported were dominatingly red and pink colors.

Lawrence et al. (2025) reported widespread auroral sightings across the United Kingdom, reaching below 54°N. Lawrence et al. (2025) did not mention color, so it is presumed that they were green auroras. Foster et al. (2024) reported a high-altitude red aurora with weaker green emission below at the Missouri Skies Observatory at 40°N. Gonzales-Esparza et al. (2024) reported citizen science observations of red auroral displays at 20 of 32 states of Mexico ranging latitudes from 26° to 38° magnetic latitude (MLAT).

Kataoka et al. (2024a) reported citizen-science observations of a red aurora during a super substorm (Tsurutani et al., 2015) that was triggered by an interplanetary shock that occurred at 1520 UT October 10, 2024. The top height of red aurora in Japan extended to ∼950 km and the red aurora shifted toward lower latitudes (down to 35°N) with increasing storm intensity (decreasing Dst index). Kataoka et al. (2025) reported an earlier citizen scientist observation from northern Japan (36°–38° MLAT) during a 1 December 2023 magnetic storm with a Dst value of only -107 nT (a very minor magnetic storm). The auroral brightness was ∼5 kR, visible by eye. This occurred during an unusually high solar wind density of >50 cm^{-3} and a high ram pressure event.

Kataoka et al. (2024b) also reported "red (O) and blue (N_2^+) aurora at extreme altitudes" during the 10–11 May 2024 superstorm. They conclude that the "blue color is caused by resonant scattering of the upwelling molecular ions". They have called this a SAR arc and have noted that there are "ray-like structures that have appeared in many of the citizen science photos".

Nanjo and Shiokawa (2024) reported two citizen scientist observations of "reddish purple or salmon pink" (instead of the usual red) auroral observations at ∼40°MLAT in Japan during the 10–11 May 2024 superstorm "recovery phase" (more will be stated about the storm "recovery phase later"). The auroras were reddish-purple up to ∼400 km altitude and occasionally blue up to at least ∼900 km. The blue dominant aurora had distinct longitudinal and field-aligned structures. Simultaneous photometric observations of the blue portion of the aurora indicated that it was due to a 4278 Å (427.8 nm) N_2^+ line. The auroras occurred during a substorm (see Shiokawa et al., 1997) within the "recovery phase" of the storm. Nanjo and Shiokawa state that the blue portion was not due to resonant scattering.

It is the purpose of this paper to report high temporal and high spatial resolution photographs taken over Braunschweig and Göttingen, Germany during the second main phase portion of the 10–11 May 2024 superstorm. Interesting features of the high time resolution of the auroral images lead us to specific conclusions concerning the generation mechanism(s) of the red-green auroras over Braunschweig and Göttingen, Germany.

Note that above simultaneous red and green aurora were noted by Foster et al. (2024). Red auroral streaks were mentioned by Kataoka et al. (2024b). We will report more concerning both of these citizen science observations.

2 Background Information

2.1 Red and Green Auroras

Red auroral lines are caused by the decay of an oxygen atom meta-stable state (^{1}D) to the ^{3}P state. This meta-stable state is long lived with a lifetime of ∼110 sec. The emissions occur at 6300 Å and lesser at 6364 Å (630.0 and 636.4 nm). The green aurora is also associated with the decay of a metastable state of oxygen atoms, from the ^{1}S state into the ^{1}D state. The mean lifetime of the ^{1}S state is ∼0.74 sec. The decay is the well-known green 5577 Å (557.7 nm) line. The auroral green line is typically the brightest line seen in auroras in the high latitude auroral zone (65° to 70° magnetic latitudes) during substorms and geomagnetic quiet intervals. The typical altitude of the green auroras is ∼130 to ∼85 km. The activation of these meta-stable states of oxygen is caused by electron collisions. The probability for the excitation into one of these states depends on the collision cross section σ. Above a few 100 eV is the so-called Bethe-regime with $\sigma \propto 1/E$, where E is the electron energy. Typical values of σ are:

Electron energy	σ[O(^{1}D)]	σ[O(^{1}S)]
20 eV (measured)	$1.5 \times 10^{-17}\mathrm{cm}^2$	$\sim 2 \times 10^{-18}\mathrm{cm}^2$
1 keV (extrapolated)	$\sim 1 \times 10^{-18}\mathrm{cm}^2$	$\sim 2 \times 10^{-19}\mathrm{cm}^2$
10 keV (extrapolated)	$\sim 2 \times 10^{-19}\mathrm{cm}^2$	$\sim 2 \times 10^{-20}\mathrm{cm}^2$

With these cross-section values we can determine the probability of an excitation per path length: $n\dot{\sigma}$ where n is the density of atoms. For example, an electron with 20 eV kinetic energy has a $\sigma \approx 10^{-17}\mathrm{cm}^2$. The oxygen atomic density at a height of 200 km is $\sim 10^{11}$ atom cm^{-3}. Thus, a path length at this height would be ∼1 cm. These results (after some further considerations) are a probability of $\sim 10^{-6}$ for an excitation of the oxygen ^{1}D state. Thus, we need many electrons to get a suitable number of excited atoms to cause bright auroral activity. The low probability furthermore implies that a single keV electron can cause many excitations. However, it is noted from the above σ values that the values decrease with increasing electron energy.

2.2 Peviously Proposed Mechanisms for Red Auroras

An important process we need to consider is quenching or collisional deexcitation, the deactivation of the oxygen meta-stable state by collisions with other atoms and molecules, for example, nitrogen. Quenching implies that the oxygen atom returns to

its ground state without emitting a photon. A typical quenching reaction is: $O(^1D) + N_2 \rightarrow O + N_2$. Thus, quenching strongly depends on the nitrogen molecular density. At heights above ∼200 km this density is low and quenching does not occur. This implies that the long-living $O(^1D)$ oxygen atoms have a high probability of emitting red photons. Below about 180 km the nitrogen density increases. Emission is no longer possible because of significant quenching of the $O(^1D)$ atom. This is the reason why red auroras are typically occurring at heights above ∼200 km. Oxygen atoms decaying from the ^1S state have much shorter lifetimes. Thus, they are not as vulnerable to quenching as from $O(^1D)$. Within a lifetime of ∼0.74 sec the chances of a stimulated oxygen atom to collide with a nitrogen molecule is low. Thus, metastable oxygen ^1S states can survive in even denser atmospheric environments. This is the reason why green auroral emissions occur much lower in the atmosphere than the red emissions. Only below a height of ∼90 km are atmospheric densities high enough to cause quenching of the $O(^1S)$ state.

The physical mechanism for the excitation of high-altitude oxygen atoms for the creation of red auroras has been debated in literature. Cole (1965) suggested that the storm-time ring current electrons and ions transfer energy to neutral particles via Coulomb collisions to heat the thermal plasma to temperatures of ∼104 K. Heat conduction down the magnetic field lines of force were proposed to create the red aurora. Rees et al. (1967) and Rees (1989) suggested precipitation of ∼1 to 4 keV electrons along geomagnetic field lines produce secondary non-ionizing electrons which excite oxygen atoms to a metastable state. Cornwall et al. (1970, 1971) suggested that during the magnetic storm recovery phases, the plasmasphere begins to physically enlarge itself from its shrunken storm-time state, bringing the high density $\sim 10^3\,\mathrm{cm}^{-3}$ thermal plasmaspheric plasma over the ring current energetic particles. This leads to an instability of the ring current ions and the growth of ion cyclotron waves. The ion cyclotron waves, then by Landau damping of the waves, accelerate thermal electrons to suprathermal energies. The suprathermal electrons excite the oxygen atoms to their metastable states. More recently, Kozyra et al. (1993) have proposed that it is energetic ring current oxygen ions which are the ultimate source for Stable Auroral Red (SAR) arcs. Collisions between these energetic ions and thermal plasmaspheric electrons energize the electrons. The energized electrons in turn stimulate the oxygen atoms to their excited metastable states.

3 The Magnetic Storm of 10–11 May 2024

Figure 1 shows the complex interplanetary causes of the 10–11 May 2024 magnetic storm. The storm main phase occurred in three primary steps with peak intensities of SYM-H $= -183$nT, -354nT and -518nT, as previously mentioned. They were caused by southward IMF Bz with intensities -40 nT, -43 nT and -71 nT (see detailed discussion in Hajra et al., 2024). The first storm main phase step was caused by sheath interplanetary southward Bz fields. The second storm main phase step was caused by MC IMF Bz southward fields. The third step was presumably due to southward Bz fields in sheath plasma. The times of the three different Braunschweig and Göttingen red auroral sightings are indicated in Figure 1g by black triangles.

Four magnetic cloud (MC) intervals were identified examining the plasma-β and IMF variations together. The times of the four MCs are: ∼20:50 UT on 10 May to ∼00:23 UT on 11 May ~~(MC1)~~ ∼03:05 to ∼07:55 UT on 11 May ~~(MC2)~~; ∼08:15

105 to ∼10:07 UT on 11 May ~~(MC3)~~; and ∼11:53 to ∼17:26 UT on 11 May ~~(MC4)~~. The MCs southward Bz created intense magnetic storms. Thus, it is possible that the Nanjo and Shiokawa (2024) red/purple and blue auroras detected during magnetic substorms also occurred during magnetic storm main phases. The storm "recovery phase" was not a pure recovery where the ring current particles were lost. Additional energetic particles were injected into the magnetosphere, indicated by the decreases in the SYM-H indices.

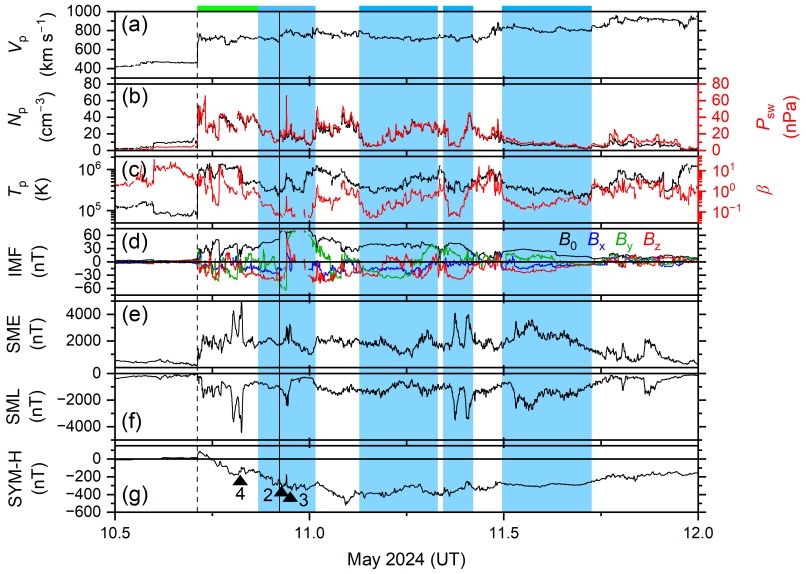


Figure 1. Solar wind/interplanetary and geomagnetic conditions during the 10–11 May 2024 storm. From top to bottom, the panels are: (a) solar wind proton speed $V_{\rm p}$, (b) proton density $N_{\rm p}$ (black, legend on the left) and ram pressure $P_{\rm sw}$ (red, legend on the right), (c) proton temperature $T_{\rm p}$ (black, legend on the left) and plasma-β (red, legend on the right), (d) interplanetary magnetic field (IMF) magnitude B_0, and B_x, B_y, and B_z components, (e) auroral electrojet index SME, (f) auroral electrojet index westward component SML, and (g) symmetric ring current index SYM-H. The solar/interplanetary parameters (a–d) have time resolution of 1 hr, and the geomagnetic indices (e–g) have time resolution of 1 min. Vertical lines indicate an interplanetary fast forward shock (dashed line) and a magnetosonic wave (not a shock; solid line) impingement times. An interplanetary sheath is marked by a green bar at the top. Four magnetic clouds (MCs) are marked by vertical blue shadings. Black triangles in the SYM-H panel indicate auroral image times. From left to right the triangles indicate red auroral images shown in Figures 4, 2, and 3, which will be shown later. The Figure is an adaptation of one in Hajra et al. (2024).

110 The photograph data to be shown soon occurred during substorms indicated by strong SME/SML indices. Image in Figure 4 occurred during a supersubstorm of intensity SML $= -4456$ nT. Photographs in Figures 2 and 3 occurred during a substorm of peak intensity SML $= -2450$ nT.

Auroras were seen over Braunschweig and Goettingen, Germany between ∼19:00 and 24:00 UT ~~(and perhaps longer)~~ on 10 May 2024. The image in Figure 2 was taken at ∼22:16 UT. Braunschweig is at an MLAT of 52.2° and an L-shell value of 2.69.

The photo was taken by a Google Pixel 7 (6.81 mm), Ultra HDR, standard zoom, f-stop 1.85 and ISO 9338. The exposure time was 6 s. Notice the stars appear as points. consistent with the fast exposure times.

Several interesting features can be noted in this closeup of the aurora shown in the figure. The red portion of the aurora is not a featureless reddish display, but there are rays in the red auroras from the upper right downward slightly to the left. This has never been reported before in scientific articles, to our knowledge. The rays in the red aurora are continued into the green aurora. The rays are enhancements in brightness. In general, the green aurora is featureless other than the rays.



Figure 2. A red and green aurora detected over Braunschweig, Germany (L-shell of 2.69) on 10 May 2024. Notice the parallel rays in both the red and green auroras. The photo was taken by Philipp Schulz at 22:16 UT. The center of the photo is pointed in the east-northeast direction. Cygnus and Lyra constellations are visible. Other than the rays, the green aurora is "featureless" in that they do not have ∼1 km width arcs or ribbons like those that occur in auroral zone (65° to 70°) green auroras.

Figure 3 shows another interesting feature of the red and green aurora taken at 22:49 UT. The view is to the north-east direction. The picture was taken by a Canon R6 Mark II with a Canon L Zoom 14–35 mm lens. A tripod was used with the lens at 16 mm, an f-stop of 4 and a 6 sec exposure. The ISO setting was 2500. Göttingen is at 51.6° MLAT and an L-shell value of 2.61.

Figure 3 shows that both the red and green rays were again enhanced brightness regions. The red rays continue down to lower altitude green rays. There is an apparent gap between the red and green aurora. The rays from the red to green auroras are present, but there is a dimming in between.



Figure 3. A red and green aurora taken over Göttingen, Germany (L-shell of 2.61). The photo was taken by Sami Solanki at 22:49 UT.

The image in Figure 4 was taken at 19:43 UT at Göttingen, Germany, some ∼2.5 to 3 hrs prior to the images of Figures 2 and 3. At the time of Figure 4, the magnetic storm main phase was less intense than during the prior figures. Figure 4 shows a different relationship between the red and green auroras. The two types of auroras are separate. There is no green aurora visible beneath the red aurora there is no red aurora above the green aurora. Rays are not visible in either green aurora or red aurora. One possible interpretation is that both the green aurora or red aurora are distant features making the viewing of rays difficult. A possible explanation of the separation of the green aurora or red aurora is that the red aurora is on magnetic field lines within the plasmasphere and the green aurora is on magnetic field lines just outside of the plasmasphere.

The auroral observations in Figures 4, 2, and 3 occurred between ∼19:00 and 23:00 UT on 10 May during the storm second main phase. The red auroral observation time in Figure 4 is indicated by the far-left triangle in Figure 1g. This corresponds to the first step of the main phase storm extending into the beginning of the second step of the main phase storm. However perhaps more important is that the time of the red and green auroral observation occurred during a supersubstorm (SSS; Tsurutani et al.,



Figure 4. A red and green aurora taken in Göttingen, Germany (L-shell of 2.61). The red aurora is in the center of the image and the green arc is on the right. The direction of the image is 288° in azimuth or the west-north-west direction. The picture was taken with a Canon EOS M, an 8 mm Fish-Eye lens, and a f-stop of 2.8. The exposure time was 8 sec. The ISO was 800. The picture was taken by Klaus Reinsch at 19:43 UT.

2015) of intensity SML $= -4456$ nT (Figure 1f) triggered by an abrupt IMF B_z southward excursion of -18 nT (Figure 1d) (see Hajra et al., 2025, for a detail discussion of all SSSs occurring during the May 2024 superstorm).

The red auroras in Figures 2 and 3 (the second and third triangles from the left in Figure 1g) occurred in the second step of the magnetic storm main phase when the SYM-H value was relatively intense. SYM-H was between -176 and -352 nT.

4 Summary of Auroral Observations

1. Modern high-speed camera images of red and green over Braunschweig and Goettingen, Germany, during the second storm main phase showed parallel linear red auroral brightness rays, indicating that they were created by precipitating energetic electrons traveling along magnetic field lines.

2. Figure 4 was taken during a supersubstorm of intensity SML $= -4456$ nT and Figures 2 and 3 were taken during an intense substorm with SML $= -2450$ nT.

3. The red auroral rays continued to lower altitude green auroral rays indicating that both the red and green auroras were caused by the same magnetospheric/ionospheric phenomenon.

4. Other than the rays/streaks in the green aurora, the aurora was diffuse. No narrow band curtains or draperies were noted. Diffuse auroras (Thorne, 2010) are caused by magnetospheric equatorial pitch angle scattering of energetic electrons into the loss cone, propagating down the magnetic fields and loss to the atmosphere.

5 Discussion

O'Brien and Moldwin (2003) construct an empirical model of the plasmapause location as a linear function of three geomagnetic indices: Kp, log AE, and log Dst. The MLT-dependence assumed a cosine function with respect to the plasmapause bulge direction. The model is an extension of the earlier model by Carpenter and Anderson (1992), and was based on over 900 plasmapause crossings of the CRRES spacecraft. We obtain from the empirical models (Eq. 3 and Table 3 in O'Brien and Moldwin, 2003) the plasmapause location using the three separate indices. For Kp $= 9$ the predicted plasmapause is in the range $L \sim 2.01$ (post-midnight sector) to $L \sim 2.68$ (post-dusk sector). For log AE (with AE $= 4098$ nT) the plasmapause is located between $L \sim 2.36$ (post-midnight) and $L \sim 2.94$ (post-dusk). For log Dst (with Dst $= -339$ nT) the plasmapause is predicted to be located between $0L \sim 2.56$ (post-midnight) and $L \sim 2.66$ (post-dusk). The estimated plasmapause location reasonably agrees with the L-shell of Braunschweig ($L \sim 2.69$) as in Fig. 2 at 22:16 UT and Göttingen ($L \sim 2.61$) as in Fig. 3 at 22:49 UT and Fig. 4 at 19:43 UT.

The observation of continuous bright rays in the red and green aurora observed over Braunschweig and Göttingen, Germany, during the 10–11 May 2024 superstorm indicate a specific auroral generation mechanism. The bright ray enhancements show that energy is directly deposited at altitudes between ∼800 km and ∼100 km (and below) by energetic electron precipitation.

This rules out the mechanism of Coulomb collision of ring current protons with plasmaspheric ions and heat conduction flowing down the magnetic field lines as proposed by Cole (1965), at least for causing the red streaks/rays. The presence of the rays in the SAR arcs is contrary to the idea of Landau damping of electromagnetic ion cyclotron waves produced by anisotropic ring current protons (Cornwall et al., 1970, 1971). The rays spatially continuing from the red aurora to the green aurora are contrary to the proposed idea that the red aurora is caused by energetic ring current oxygen ions (Kozyra et al., 1993). It is well known that green aurora rays are produced by energetic precipitating electrons (Lummerzheim, 2007).

5.1 Electron Acceleration Mechanism

Rees et al. (1967) proposed that ∼1 to 4 keV precipitating electrons are creating secondary electrons which then stimulate oxygen atoms into their elevated metastable states. Such low energy electrons are "monoenergetic" (Evans, 1974) and are now known to be accelerated in double layers a few R_{E} (Earth radii) above the surface of the Earth (Lemaire and Scherer, 1974; Carlson and Kelley, 1977; Block, 1978). Hasegawa (1976) and Goertz and Boswell (1979) suggest that a parallel electric field component of the kinetic Alfvén wave is causing the electron acceleration. It is noted that the parallel electric field component of the kinetic Alfvén wave is sustained by the electron inertia terms in Goertz and Boswell (1979) mechanism and by the finite ion Larmor radius effects in Hasegawa (1976) mechanism. Both dispersive mechanisms play important roles in the auroral

acceleration region. At higher altitudes finite ion Larmor radius effects Hasegawa (1976) dominates whereas at lower altitudes the electron inertial effects Goertz and Boswell (1979) dominates. The precipitation from acceleration in double layers forms discrete auroras of ∼km width arcs, not diffuse auroras. Thus, the Rees et al. (1967) mechanism can possibly be discounted.

5.2 Energetic Electrons in the Plasmasphere

The fact that these red auroral observations were made during an intense magnetic storm main phase is suggestive that the energetic electron source is inside the high plasma density plasmasphere. This is the general conclusion of the plasmasphere and instabilities within playing a major role in red auroras, suggested in the review of Kozyra et al. (1997). The precipitation of broadband energetic electrons of ∼30 eV to 30 keV associated with substorms during magnetic storms by Shiokawa et al. (1997) is consistent with this hypothesis.

It has been speculated that substorm convection electric fields are separate and distinct from magnetic storm convection electric fields (Tsurutani and Gonzalez, 2007). The plasmapause location estimated at $L = 2.6$ supports the mechanism that the substorm electric fields have injected energetic particles into the high plasma density plasmasphere, leading to the red and green auroras.

If the source of energetic electrons causing the red and green aurora are pitch angle scattered ring current electrons, what are the waves that scatter the ring current electrons into the loss cone and the instability that creates the plasma waves? What is detected at and near the plasmapause during strong geomagnetic activity are magnetosonic waves generated by an ion ring distribution instability (Gurnett, 1976; Perraut et al., 1982; Boardsen et al., 1992; Horne et al., 2000; Santolík et al., 2002; Meredith et al., 2008; Pokhotelov et al., 2008; Němec et al., 2013). Tsurutani et al. (2014) showed details of magnetosonic waves during a substorm at local midnight. The waves were linear polarization with exceptionally large $E_{\rm w} = \pm 25\,{\rm mV/m}$ electric oscillations perpendicular to B_0 and large $B_{\rm w} = \pm 1\,{\rm nT}$ magnetic components parallel to B_0. Plasmaspheric hiss was detected away from the magnetic equator. It is possible that both the magnetosonic wave electric field oscillations and the plasmaspheric hiss are leading to energetic electron pitch angle diffusion into the loss cone.

If the precipitating electrons are indeed deeply injected substorm particles, it is possible that there will be a high energy ∼100 to 200 keV precipitating component and bremsstrahlung X-rays produced which may cause interesting ionospheric and atmospheric effects below.

6 Final Comments

In this paper, we have discussed short duration red and green mid-latitude auroral events that have been detected during intense substorms during a storm main phase. The substorms occurred during the second step of the main phase of a magnetic storm. This is the first paper showing that red auroras and green auroras were connected (by the continuous streaks).

These events are probably not the same type of middle latitude red auroras as those that are called "Stable Auroral Red" aurora (SAR arcs) that last for "tens of hours" as was mentioned by Roach and Roach (1963) (although Kataoka et al. (2024b) has called these SAR arcs). There may be several different types of red auroras. Belon and Clark (1959) reported on spectroscopic observations on the 10-11 February 1958 "great red aurora". They detected 5577 Å and 6584 Å emissions as well as the red lines. Rees and Deehr (1961) reported spectrophotomic observations of a high altitude red auroral arc that occurred on 27 November 1959. The intensity of the 6300 Å line was 66.7 kR, unusually intense (visible by eye). They reported that this arc was purely 6300-6364 Å lines and the N_2^+ NG bands "with other usual auroral emission features being noticeably absent". Mendillo et al. (2016) studied what they called a Stable Auroral Red (SAR) arc with "several superimposed patches of emission in two oxygen lines (with a 6300 Å/5577 Å) ratio of ∼40." Mendillo et al. (2016) also stated: "We find no evidence for highly localized heating effects, but rather evidence from GPS satellites supporting low-energy electron precipitation as the SAR arc modulating mechanism." Earlier, Rassoul et al. (1993) determined a 6300 Å/5577 Åratio of only 3.8 with "other weaker emissions that were characteristic of heavy particle auroras and can be attributed to energetic (keV) ions and neutral atoms from the ring current."

It thus seems highly likely that there are many types of middle latitude red auroras. It will be interesting to determine if there are 1) pure red arcs without green aurora below, 2) all red arcs have green aurora below, or 3) if both possibilities exist. It will also be interesting to know if there are bremsstrahlung X-ray emissions produced in red-green auroras.

Future citizen science reports of close up high spatial and high temporal (integration times $<$ 10 second) results of red auroras will be useful for understanding the physical mechanism of the aurora. If there are no streaks and no green aurora below, the physical mechanism for the aurora will be different than the one concluded here. Although confirming that the mechanism is different (from this paper), it will be extremely difficult/impossible? to determine which possible mechanism is the correct one.

Data availability. The near-Earth solar wind plasma and IMF data are obtained from NASA's OMNIWeb Plus database https://omniweb.gsfc.nasa.gov/. The 1-hr and 1-min data can be directly downloaded from the pages: https://omniweb.gsfc.nasa.gov/form/dx1.html and https://omniweb.gsfc.nasa.gov/form/omni_min.html, respectively, by specifying start and stop times, and required plasma and IMF parameters.

Author contributions. Conceptualization: Bruce T. Tsurutani

Data curation: Philipp Schulz, Sami Solanki, Klaus Reinsch, Rajkumar Hajra, Bruce T. Tsurutani

Formal analysis: Bruce T. Tsurutani, Rajkumar Hajra, Gurbax S. Lakhina, Karl-Heinz Glassmeier, Masatomi Iizawa, Richard B. Horne, Yasuhito Narita, Ingo von Borstel, Volker Bothmer

Funding acquisition: Rajkumar Hajra

Investigation: Bruce T. Tsurutani, Gurbax S. Lakhina, Rajkumar Hajra, Yasuhito Narita, Richard B. Horne, Masatomi Iizawa, Ingo von Bors-

tel, Volker Bothmer, Karl-Heinz Glassmeier, Klaus Reinsch, Philipp Schulz, Sami Solanki

Methodology: Bruce T. Tsurutani, Rajkumar Hajra, Gurbax S. Lakhina, Karl-Heinz Glassmeier, Richard B. Horne, Masatomi Iizawa

Resources: Philipp Schulz, Sami Solanki, Klaus Reinsch, Rajkumar Hajra, Bruce T. Tsurutani, Volker Bothmer, Ingo von Borstel

Supervision: Bruce T. Tsurutani, Rajkumar Hajra, Yasuhito Narita

Validation: Bruce T. Tsurutani, Gurbax S. Lakhina, Rajkumar Hajra, Yasuhito Narita, Richard B. Horne, Masatomi Iizawa, Ingo von Borstel, Volker Bothmer, Karl-Heinz Glassmeier, Klaus Reinsch, Philipp Schulz, Sami Solanki

Visualization: Philipp Schulz, Sami Solanki, Klaus Reinsch, Volker Bothmer, Ingo von Borstel

Writing – original draft: Bruce T. Tsurutani

Writing – review & editing: Bruce T. Tsurutani, Gurbax S. Lakhina, Rajkumar Hajra, Yasuhito Narita, Richard B. Horne, Masatomi Iizawa, Ingo von Borstel, Volker Bothmer, Karl-Heinz Glassmeier, Klaus Reinsch, Philipp Schulz, Sami Solanki Writing – revision: Bruce T. Tsurutani, Yasuhito Narita

Competing interests. Conflict of Interest: The authors declare that the research was conducted in the absence of any commercial or financial relationships that could be construed as a potential conflict of interest.

Acknowledgements. The work of R. H. is funded by the "Hundred Talents Program" of the Chinese Academy of Sciences (CAS), and the "Excellent Young Scientists Fund Program (Overseas)", and the "Research Fund for International Excellent Young Scientists" (grant number: W2532030) of the National Natural Science Foundation of China (NSFC). Sadly our friend and colleague Volker Bothmer passed away just before this paper was published. We would like to dedicate this paper to his memory.

References

Abraham-Shrauner, B.: Determination of magnetohydrodynamic shock normals. J. Geophys. Res. 77, 736–739, 1972. https://doi.org/10.1029/JA077i004p00736

Barbier, D.: L'activite aurorale aux basses latitudes. Annales de Geophysique, 14, 334–355, 1958.

Belon, A. E. and Clark, K. C.: Spectroscopic observations of the great aurora of 10 February 1958– II. Unusual atomic features, J. Atmos. Terr. Phys. 16, 220–227, 1959. https://doi.org/10.1016/0021-9169(59)90070-4

Block, L. P.: A double layer review. Astrophys. Space Sci., 55, 59–83, 1978. https://doi.org/10.1007/BF00642580

Boardsen, S. A., Gallagher, D. L., Gurnett, D. A., Peterson, W. K., and Green, J. L.: Funnel-shaped, low-frequency equatorial waves. J. Geophys. Res. Space Physics, 97, 14,967–14,976, 1992. https://doi.org/10.1029/92JA00827

Carlson, C. W., and Kelley, M. C.: Observation and interpretation of particle and electric field measurements inside and adjacent to an active auroral arc. J. Geophys. Res. 82, 2349–2360, 1977. https://doi.org/10.1029/JA082i016p02349

Carpenter, D. L. and Anderson, R. R.: An ISEE/whistler model of equatorial electron density in the magnetosphere, J. Geophys. Res. Space Physics, 97, 1097–1108, 1992. https://doi.org/10.1029/91JA01548

Cole, K. D.: Stable auroral red arcs, sinks for energy of $D_{\rm st}$ main phase. J. Geophys. Res., 70, 1689–1706, 1965. https://doi.org/10.1029/JZ070i007p01689

Cornwall, J. M., Coroniti, F. V., and Thorne, R. M.: Turbulent loss of ring current protons. J. Geophys. Res., 75, 4699–4709, 1970. https://doi.org/10.1029/JA075i025p04699

Cornwall, J. M., Coroniti, F. V., and Thorne, R. M.: Unified theory of SAR arc formation at the plasmapause. J. Geophys. Res., 76, 4428–4445, 1971. https://doi.org/10.1029/JA076i019p04428

Evans, D. S.: Precipitating electron fluxes formed by a magnetic field aligned potential difference. J. Geophys. Res., 79, 2853–2858, 1974. https://doi.org/10.1029/JA079i019p02853

Foster, J. C., Erickson, P. J., Nishimura, Y., Zhang, S. R., Bush, D. C., Coster, A. J., et al.: Imaging the May 2024 extreme aurora with ionospheric total electron content, Geophys. Res. Lett., 51, e2024GL111981, 2024. https://doi.org/10.1029/2024GL111981

Goertz, C. K., and Boswell, R. W.: Magnetosphere-ionosphere coupling, J. Geophys. Res., 84, 7239–7246, 1979.

Gonzalez-Esparza, J. A., Sanchez-Garcia, E., Sergeeva, M., Corona-Romero, P., Gonzalez-Mendez, L. X., Valdes-Galicia, J. F., et al.: The Mother's Day geomagnetic storm on 10 May 2024: Aurora observations and low latitude space weather effects in Mexico, Space Weather, 22, e2024SW004111, 2024. https://doi.org/https://doi.org/10.1029/2024SW004111

Grandin, M., Bruus, E., Ledvina, V. E., Partamies, N., Barthelemy, M., Martinis, C., et al.: The Gannon Storm: citizen science observations during the geomagnetic superstorm of 10 May 2024. Geosci. Comm., 7, 297–316, 2024. https://doi.org/10.5194/gc-7-297-2024

Gurnett, D. A., Plasma wave interactions with energetic ions near the magnetic equator. J. Geophys. Res., 81, 2765–2770, 1976. https://doi.org/10.1029/JA081i016p02765

Hajra, R., Tsurutani, B. T., Lakhina, G. S., Lu, Q., and Du, A.: Interplanetary causes and impacts of the 2024 May superstorm on the geosphere: An Overview. Astrophys. J., 974, 264. 2024. https://doi.org/10.3847/1538-4357/ad7462

Hajra, R., Tsurutani, B. T., Lu, Q., Du, A., and Lakhina, G. S.: Supersubstorms during the May 2024 superstorm. J. Space Weather Space Clim., 15, 51, 2025. https://doi.org/10.1051/swsc/2025047

Hasegawa, A.: Particle acceleration by MHD surface wave and formation of aurora. J. Geophys. Res, 81, 5083–5090. 1976. https://doi.org/10.1029/JA081i028p05083

Horne, R. B., Wheeler, G. V., and Alleyne, H. St. C. K.: Proton and electron heating by radially propagating fast magnetosonic waves. J. Geophys. Res. Space Physics, 105, 27,597–27,610. 2000. https://doi.org/10.1029/2000JA000018

~~Hugoniot, H.: Mémoire sur la propagation des mouvements dans les corps et spécialement dans les gaz parfaits (premiŕe partie). Journal de l'École Polytechnique, 57, 3–97, 1887.~~

~~Hugoniot, H.: Mémoire sur la propagation des mouvements dans les corps et spécialement dans les gaz parfaits (deuxiňe partie), Journal de l'Éole Polytechnique, 58, 1–125, 1889.~~

Kataoka, R., Miyoshi, Y., Shiokawa, K., Nishitani, N., Keika, K., Amano, T. and Seki, K.: Magnetic storm-time red aurora as seen from Hokkaido, Japan on 1 December 2023 associated with high-density solar wind, Geophys. Res. Lett., 51, e2024GL108778, 2024a. https://doi.org/10.1029/2024GL108778

Kataoka, R., Reddy, S. A., Nakano, S., Pettit, J., and Nakamura, Y.: Extended magenta aurora as revealed by citizen science. Scientific Reports, 14, 25849. 2024b. https://doi.org/10.1038/s41598-024-75184-9

Kataoka, R., Nakano, S., Uchino, S. and Reddy, S.A. Extended red aurora associated with super substorm igniting the October 10, 2024 magnetic storm as revealed by citizen science, Earth Planets Space, 77, 64, 2025. https://doi.org/10.1186/s40623-025-02178-w.

Kozyra, J. U., Chandler, M. O., Hamilton, D. C., Peterson, W. K., Klumpar, D. M., Slater, D. W., et al.: The role of ring current nose events in producing stable auroral red arc intensifications during the main phase: Observations during the September 19–24, 1984, Equinox Transition Study. J. Geophys. Res. Space Physics, 98, 9267–9283. 1993. https://doi.org/10.1029/92JA02554

Kozyra, J. U., Nagy, A. F., and Slater, D. W.: High-altitude energy source(s) for stable auroral red arcs. Rev. Geophys., 35, 155–190, 1997. https://doi.org/10.1029/96RG03194

Lawrence, E., Beggan, C. D., Richardson, G. S., Reay, S., Thompson, V., Clarke, E., et al.: The geomagnetic and geoelectric response to the May 2024 geomagnetic storm in the United Kingdom. Frontiers in Astronomy and Space Sciences, 12, 1550923, 2025. https://doi.org/10.3389/fspas.2025.1550923

Lemaire, J., and Scherer, M.: Ionosphere-plasmasheet field-aligned currents and parallel electric fields. Planet. Space Sci., 22, 1485–1490, 1974. https://doi.org/10.1016/0032-0633(74)90013-0

Lummerzheim, D.: Modeling and forecasting aurora. Comp. Sci. Engineer., 9, 53–61, 2007. https://doi.org/10.1109/MCSE.2007.103

Mendillo, M., Finan, R., Baumgardner, J., Wroten, J., Martinis, C., and Casillas, M.: A stable auroral red (SAR) arc with multiple emission features, J. Geophys. Res. Space Physics, 121. 10,564–10,577, 2016. https://doi.org/10.1002/2016JA023258

Meredith, N. P., Horne, R. B., and Anderson, R. R.: Survey of magnetosonic waves and proton ring distributions in the Earth's inner magnetosphere. J. Geophys. Res. Space Physics, 113, A06213, 2008. https://doi.org/10.1029/2007JA012975

Nanjo, S. and Shiokawa, K.: Spatial structures of blue low-latitude aurora observed from Japan during the extreme geomagnetic storm of May 2024. Earth, Planets Space, 76, 156, 2024. https://doi.org/10.1186/s40623-024-02090-9

Němec, F., Santolík, O., Pickett, J. S., Hrbáčková, Z., and Cornilleau-Wehrlin, N.: Azimuthal directions of equatorial noise propagation determined using 10 years of data from the Cluster spacecraft. J. Geophys. Res. Space Physics, 118, 7160–7169, 2013. https://doi.org/10.1002/2013JA019373

O'Brien, T. P. and Moldwin, M. B.: Empirical plasmapause models from magnetic indices. Geophys. Res. Lett., 30, 2002GL016007, 2003. https://doi.org/10.1029/2002GL016007

Perraut, S., Roux, A., Robert, P., Gendrin, R., Sauvaud, J. A., Bosqued, J. M., et al.:. A systematic study of ULF waves above F_{H+} from GEOS 1 and 2 measurements and their relationships with proton ring distributions, J. Geophys. Res. Space Physics, 87, 6219–6236, 1982.. https://doi.org/10.1029/JA087iA08p06219

Pokhotelov, O. A., Sagdeev, R. Z., Balikhin, M. A., Onishchenko, O. G., and Fedun, V. N.: Nonlinear mirror waves in non-Maxwellian space plasmas. J. Geophys. Res. Space Physics, 113, 2007JA012642, 2008. https://doi.org/10.1029/2007JA012642

Rankine, W. J. M.: On the thermodynamic theory of waves of finite longitudinal disturbance. Phil. Trans. Royal Soc. London, 160, 277–288, 1870. https://doi.org/10.1098/rstl.1870.0015

Rassoul, H. K., Rohrbaugh, R. P., Tinsley, B. A., and Slater, D. W.: Spectrometric and photometric observations of low-latitude aurorae. J. Geophys. Res. Space Physics, 98, 7695–7709, 1993. https://doi.org/10.1029/92JA02269

Rees, M. H.: Physics and Chemistry of the Upper Atmosphere (1st ed.). Cambridge University Press, 1989. https://doi.org/10.1017/CBO9780511573118

Rees, M. H. and Deehr, C. S., The aurora of 27 November 1959 at College, Alaska including observations of a high altitude red arc, Planet. Space Sci., 8, 49–58, 1961. https://doi.org/10.1016/0032-0633(61)90155-6

Rees, M. H., Walker, J. C. G., and Dalgarno, A.: Auroral excitation of the forbidden lines of atomic oxygen. Planet. Space Sci., 15, 1097–1110, 1967. https://doi.org/10.1016/0032-0633(67)90096-7

Roach, F. E., and Marovich, E.: A monochromatic low-latitude aurora. J. Res. Nat. Bureau Standard, Section D: Radio Propagation, 63D, 297, 1959. https://doi.org/10.6028/jres.063D.029

Roach, F. E., and Roach, J. R.: Stable 6300 Åauroral arcs in mid-latitudes. Planet. Space Sci., 11, 523–549, 1963. https://doi.org/10.1016/0032-0633(63)90076-X

Santolík, O., Pickett, J. S., Gurnett, D. A., Maksimovic, M., and Cornilleau-Wehrlin, N.: Spatiotemporal variability and propagation of equatorial noise observed by Cluster. J. Geophys. Res. Space Physics, 107, SMP 43, 2002. https://doi.org/10.1029/2001JA009159

Schriver, D., Ashour-Abdalla, M., Strangeway, R. J., Richard, R. L., Klezting, C., Dotan, Y., and Wygant, J.: FAST/Polar conjunction study of field-aligned auroral acceleration and corresponding magnetotail drivers. J. Geophys. Res. Space Physics, 108, COA 21. 2003. https://doi.org/10.1029/2002JA009426

Shiokawa, K., Meng, C.-I, Reeves, G. D., Rich, F. J., and Yumoto, K.: multievent study of broadband electrons observed by the DMSP satellites and their relation to red aurora observed at midlatitude stations, J. Geophys. Res. Space Physics, 102, 14237–14253, 1997. https://doi.org/10.1029/97JA00741

Shiokawa, K., Ogawa, T., and Kamide, Y.: Low-latitude auroras observed in Japan: 1999–2004. J. Geophys. Res., 110, A05202, 2005. https://doi.org/10.1029/2004JA010706

Spogli, L., Alberti, T., Bagiacchi, P., Cafarella, L., Cesaroni, C., Cianchini, G., et al.: The effects of the May 2024 Mother's Day superstorm over the Mediterranean sector: from data to public communication. Annals of Geophysics, 67, PA218, 2024. https://doi.org/10.4401/ag-9117

Thorne, R. M.: Radiation belt dynamics: The importance of wave-particle interactions, Geophys. Res. Lett., 37, L22107, 2010. https://doi.org/10.1029/2010GL044990

Tsurutani, B. T., and Gonzalez, W. D.: A new perspective on the relationship between substorms and magnetic storms, Advances in Geosciences, Vol. 8, Solar Terrestrial, pp. 25–45, 5 Toh Tuck Link, Singapore 596224: World Scientific Publishing, 2007. https://doi.org/10.1142/9789812708939_0002

Tsurutani, B. T., Falkowski, B. J., Pickett, J. S., Verkhoglyadova, O. P., Santolik, O., and Lakhina, G. S.: Extremely intense ELF magnetosonic waves: A survey of polar observations. J. Geophys. Res. Space Physics, 119, 964–977. 2014. https://doi.org/10.1002/2013JA019284

Tsurutani, B. T., Hajra, R., Echer, E., and Gjerloev, J. W.: Extremely intense ($\mathrm{SML} \leq -2500\ \mathrm{nT}$) substorms: isolated events that are externally triggered? Ann. Geophys., 33, 519–524, 2015. https://doi.org/10.5194/angeo-33-519-2015